

Effect of magnesium oxide adhesion layer on resonance behavior of plasmonic nanostructures

Cite as: Appl. Phys. Lett. **116**, 241601 (2020); <https://doi.org/10.1063/5.0008665>

Submitted: 25 March 2020 . Accepted: 30 May 2020 . Published Online: 15 June 2020

Parinaz Sadri-Moshkenani , Mohammad Wahiduzzaman Khan, Md. Shafiqul Islam, Eric Montoya , Ilya Krivorotov, Nader Bagherzadeh, and Ozdal Boyraz 



View Online



Export Citation



CrossMark

ARTICLES YOU MAY BE INTERESTED IN

[All-fiber focused beam generator integrated on an optical fiber tip](#)

Applied Physics Letters **116**, 241102 (2020); <https://doi.org/10.1063/5.0007022>

[Surface plasmon coupling for selectively enhanced random lasing in periodically patterned silver columnar thin film metamaterials](#)

Applied Physics Letters **116**, 241902 (2020); <https://doi.org/10.1063/5.0010413>

[Spin-resolved near-field scanning optical microscopy for mapping of the spin angular momentum distribution of focused beams](#)

Applied Physics Letters **116**, 241107 (2020); <https://doi.org/10.1063/5.0004750>

Lock-in Amplifiers
up to 600 MHz



Watch



Effect of magnesium oxide adhesion layer on resonance behavior of plasmonic nanostructures

Cite as: Appl. Phys. Lett. **116**, 241601 (2020); doi: [10.1063/5.0008665](https://doi.org/10.1063/5.0008665)

Submitted: 25 March 2020 · Accepted: 30 May 2020 ·

Published Online: 15 June 2020






View Online



Export Citation



CrossMark

Parinaz Sadri-Moshkenani,^{1,a)}  Mohammad Wahiduzzaman Khan,¹ Md. Shafiqul Islam,¹ Eric Montoya,² 
Ilya Krivorotov,² Nader Bagherzadeh,¹ and Ozdal Boyraz¹ 

AFFILIATIONS

¹Department of Electrical Engineering and Computer Science, University of California Irvine, Irvine, California 92697, USA

²Department of Physics and Astronomy, University of California Irvine, Irvine, California 92697, USA

^{a)} Author to whom correspondence should be addressed: psadrimo@uci.edu

ABSTRACT

The magnesium oxide (MgO) adhesion layer is proposed to avoid adverse effects of lossy metallic adhesion layers in thin film plasmonic nanostructures. Such adverse effects can be in the form of resonance broadening and a decrease in the resonance magnitude. We fabricate and test the quality of MgO adhesion layers and determine its optical properties through ellipsometry measurements. We also provide the plasmonic response of various plasmonic nanostructures (nanohole array, nanodisk array, dimer nanohole array, and bowtie slot antenna array) with a MgO adhesion layer and conventional adhesion layers including titanium (Ti), chromium (Cr), tantalum (Ta), and indium tin oxide (ITO). Our results show that unlike conventional adhesives, MgO has almost no adverse effect on the plasmonic resonance of the designed nanostructures.

Published under license by AIP Publishing. <https://doi.org/10.1063/5.0008665>

Plasmonic nanostructures, with the ability to show strong field localization, have a wide variety of applications, including biosensing and chemical sensing and thermoplasmonic applications.^{1–6} In such applications, gold (Au) and silver are commonly used as the plasmonic metal. Since they are both noble metals, there is a need for an adhesion layer to ensure firm bonding between the metal layer and the substrate. As a common solution to the adhesion problem, metal layers such as chromium (Cr), titanium (Ti), and tantalum (Ta) can be used. However, they adversely affect the plasmonic resonance of the metallic nanostructures. High losses induced by these adhesion metals usually have a significant damping effect, which results in resonance broadening and a decrease in its magnitude. As a result, these adverse effects decrease the performance of the plasmonic structure.^{7–13}

To avoid such degradation caused by the adhesion layer, some papers have suggested using oxides such as indium tin oxide (ITO), TiO₂, and Cr₂O₃ as adhesion layers,^{7,14–16} or a molecular linker,^{17,18} which are all low-loss materials at optical wavelengths. Specifically, preparing a molecular linker adds a few extra steps to the fabrication process as well as requiring a long deposition time. Another approach is to modify the fabrication process to achieve less overlap between plasmonic hotspots and the metallic adhesion layer, as presented in Ref. 19, through a more complicated fabrication called the angular evaporation technique.

In this manuscript, we propose magnesium oxide (MgO) low-loss adhesion layers and study the impact on the plasmonic structures. Recently, we had demonstrated that MgO can be a low-loss alternative to the conventional adhesion layers made of Cr, Ti, Ta, and other low-loss adhesion layers proposed in the literature so far.²⁰ Here, we provide detailed information on deposition and testing of the MgO adhesion layers. Furthermore, we perform a theoretical study on various plasmonic nanostructures and compare their performance in terms of resonance broadening and resonance magnitude reduction when they are fabricated with MgO and conventional adhesion layers. Specifically, nanohole arrays, nanodisk arrays, dimer nanohole arrays, and bowtie slot antenna arrays are designed for such comparison.^{21–24} In particular, we observe a large impact on the device performance when there is a larger overlap between the electric field and the adhesion layer.

In order for the adhesion material to be an acceptable choice, its adhesion performance should be tested. We fabricated two approximately $10 \times 10 \text{ mm}^2$ samples on Si100/SiO_x(100 nm) substrate as: substrate/Au(30 nm), and substrate/MgO(3 nm)/Au(30 nm). Deposition of thin films was performed by magnetron sputtering in 2 mTorr (0.27 Pa) of Ar process gas. The base pressure of the system was below 2×10^{-8} Torr (2.7×10^{-6} Pa). Au layers were deposited by d.c. sputtering, and the dielectric MgO layer was deposited through

r.f. sputtering. It was observed through SEM images [Figs. 1(b) and 1(c)] that the deposited Au layers are polycrystalline in both cases.

We use the sonication technique^{25,26} to test the adhesion of the Au layer of the fabricated samples as it is one of the harshest steps that plasmonic devices experience during fabrication or cleaning. The results are qualitative and binary, and so we can determine whether or not the devices will survive the fabrication process. We placed the samples in separate beakers of isopropyl alcohol and sonicated them. After ~ 15 min, the Au layer in the first sample was observed by the eye to be exfoliating near the edges of the wafer. The second sample [substrate/MgO(3 nm)/Au(30 nm)] showed no signs of exfoliating. At this point, we tested our samples by performing a visual inspection of the two samples through optical microscope imaging as well as scanning electron microscopy (SEM) images (Fig. 1). Continuing the sonication for 5 more hours, for the sample without the MgO adhesion layer, the gold layer was completely exfoliated, while the one with the MgO adhesion layer showed no change. This shows that the thin MgO layer creates a strong adhesion between the Au layer and the substrate. We repeated this test a second time, and a similar outcome was observed.

To demonstrate the mechanical stability of the MgO adhesion layer specifically for nanoparticles, we present our fabrication of a nanohole array and a dimer nanohole array fabricated on a stack of gold and MgO [quartz substrate/MgO(3 nm)/Au(60 nm)/MgO(6 nm)/Au(5 nm)]. We used a single layer positive tone e-beam resist poly(methyl methacrylate) (PMMA 495A4) of 250 nm by spin coating it on our sample at 3000 rpm. After spin coating, the resist was pre-baked at 180°C for 15 min. Then, electron beam exposure was done at 100 kV with a dose level of $1100\ \mu\text{C}/\text{cm}^2$ (Vistec EBPG 5000+ES E-beam Writer). Then, the resist was developed in standard MIBK:IPA 1:3 solution for 45 s, followed by IPA rinse for 30 s and N₂ blow dry. Afterward, Ar⁺ ion milling was used to etch the exposed part of the sample and create the nanohole patterns. The resist was removed by leaving the sample in 60°C acetone for 45 min, followed by a brief sonication of less than 15 s. Then, the sample was rinsed with IPA, with another brief sonication, followed by HPLC water rinse for ~ 45 s

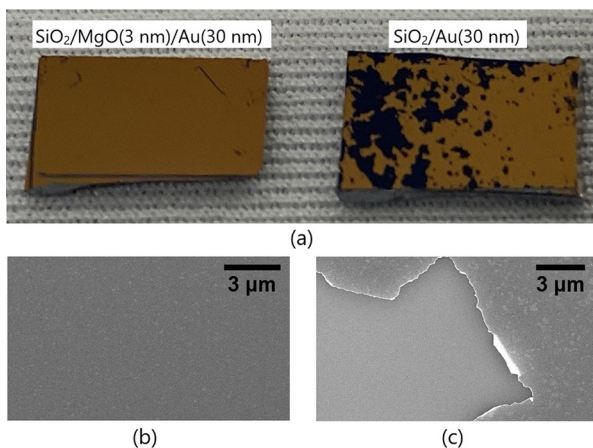


FIG. 1. MgO adhesion test samples after 15 min of sonication: (a) optical image of Au samples without and with the MgO adhesion layer. (b) SEM image of part of the sample with the MgO adhesion layer and (c) with no adhesion layer. After 5 h of sonication, the sample on the left showed no change, while for the sample on the right, the Au layer was completely removed.

and N₂ blow dry. The SEM images of the fabricated nanohole array and dimer nanohole array are shown in Fig. 2. It can be seen from the SEM images that the nanoholes have smooth circular shapes as expected, despite the multiple sonications during the fabrication process. This shows that the MgO adhesion layer creates a high enough mechanical stability for the nanostructures to survive the fabrication process. It should be noted that the affinity of MgO to water is known.²⁷ However, in a plasmonic device where the MgO adhesion layer coated with noble metals or any other stable material, water exposure and potential damage will be minimized. Applications that require devices where MgO has extensive exposure should be aware of potential damage.

Optical properties of thin-film materials can be very different from their bulk properties because of electron scattering at the film boundary.^{28–34} To account for such effects, we performed ellipsometry measurements on a 5 nm MgO thin film, which is thick enough to achieve strong adhesion. Furthermore, as an example of metallic adhesion layers to compare with, we performed ellipsometry measurements on a Ta thin film since Ta is used as a common adhesion layer, and it is particularly important for magneto-plasmonic devices.¹¹ These data will be used in our simulations presented later in this manuscript. Two samples were prepared on the quartz substrate as quartz substrate/MgO(5 nm) and quartz substrate/Ta(5 nm)/Au(2 nm), where the gold layer deposited on top of the Ta layer is to protect it from oxidation. The deposition technique for Au and MgO was the same as the ellipsometry samples. For Ta, the deposition was performed by d.c. sputtering at the same gas pressure as Au.

The plots in Fig. 3 represent the thin-film material data obtained through ellipsometry for MgO and Ta, as well as their bulk optical properties from Refs. 35 and 36. Measurements were performed at an incident angle of 70° for the wavelength range of 530 nm–750 nm. For each measurement, an average of 30 scans was taken for ensuring accuracy of the results. The Cauchy dispersion equation was assumed as the dispersion model, and the coefficients were obtained to best fit the measurement data. Another set of spectroscopic measurements was performed using a Cary-7000 Universal Measurement Spectrophotometer, which showed that the Cauchy coefficients obtained from the ellipsometry measurements can give a close estimate of optical properties of the thin films up to a wavelength of 900 nm. Therefore, the plots presented here include wavelength ranges up to $\lambda = 900$ nm. Here, a translucent tape was placed on the backside of the quartz substrate of both samples prior to the ellipsometry measurements to reduce the backside reflections. For the case of MgO, however, the backside reflection was not completely suppressed because of its extreme transparency. Therefore, the calculated

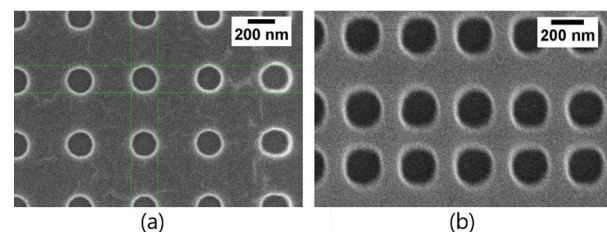


FIG. 2. SEM image of the fabricated nanostructures using the MgO adhesion layer: (a) nanohole array and (b) dimer nanohole array.

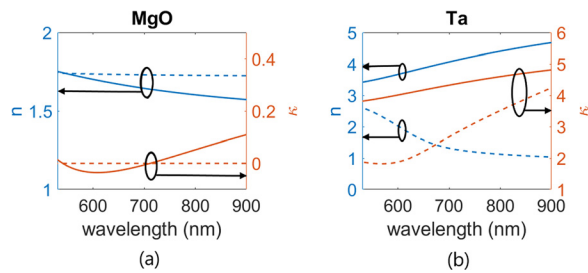


FIG. 3. Optical properties of 5 nm thin films obtained from ellipsometry measurements (solid lines) vs bulk optical properties from Refs. 35 and 36 (dashed lines) for (a) MgO and (b) Ta (n : refractive index and κ : extinction coefficient).

extinction coefficient of the MgO thin film shows a negligible negative value at shorter wavelengths, which we approximate to zero for simulations discussed later in this manuscript.

Adhesion layers can adversely affect the performance of plasmonic nanostructures and may manifest their effect on the plasmonic resonance spectrum as linewidth broadening and resonance magnitude reduction. Here, we show how much an MgO adhesion layer affects the plasmonic resonance of different plasmonic nanostructures, compared to Ta, Cr, Ti, and ITO adhesion layers to support the idea of MgO as an alternative adhesion layer for plasmonic devices.

Four different plasmonic nanostructures are designed for our study: nanohole arrays, nanodisk arrays, dimer nanohole arrays, and bowtie slot antenna arrays,^{21–24} using finite element method (FEM) simulations. The nanostructures are designed on a 60 nm gold film as the plasmonic metal and a SiO₂ substrate ($n = 1.45$ ³⁷) except for the nanodisk array where a 20 nm gold layer is considered for the design. The adhesion layer thickness is set to 5 nm, and the material data for gold are taken from Ref. 38. Both the gold layer and the adhesion layer are assumed to be fully etched in the simulations.

The unit cell schematics and the dimensions of each nanostructure are shown in Fig. 4. Dimensions are designed to achieve plasmonic resonance at 710 nm. The transmission spectra for the designed nanostructures are included in the plots of Fig. 5 (solid lines without markers). Each nanostructure, depending on its geometry, supports a specific type of plasmonic resonance. For the designed nanohole array,

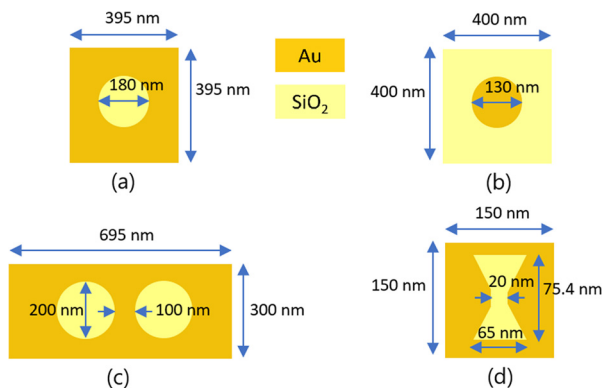


FIG. 4. Unit cell schematic and dimensions for the designed plasmonic nanostructures: (a) nanohole array, (b) nanodisk array, (c) dimer nanohole array, and (d) bowtie slot antenna array.

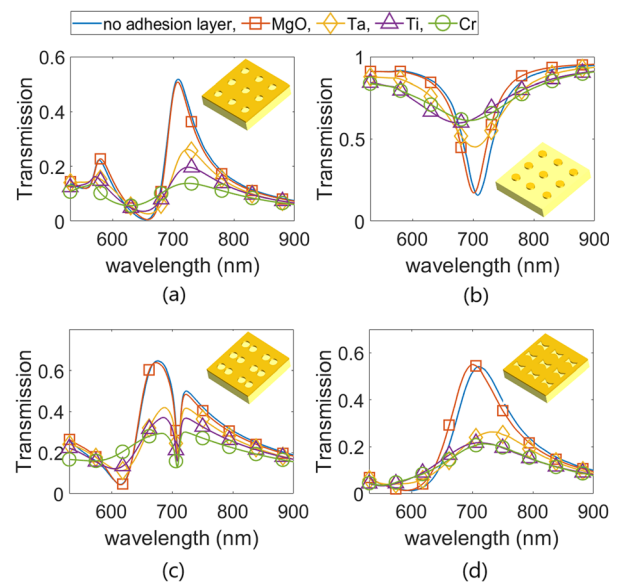


FIG. 5. Transmission spectra without and with different adhesion layers of 5 nm thickness, considering bulk optical properties of adhesion material for (a) nanohole array, (b) nanodisk array, (c) dimer nanohole array, and (d) bowtie slot antenna array.

the plasmonic resonance is mainly based on a surface plasmon polariton (SPP) mode, which is a propagating mode, appearing as a peak in the transmission spectrum, and specifically for this design, it is the SPP mode localized at the substrate/Au interface. The resonance for the dimer nanohole array is based on an SPP mode coupled with a Rayleigh–Wood Anomaly (WA) mode (at the Au/air interface), creating a Fano resonance, showing up as a dip in its transmission spectrum. Bowtie slot antenna arrays and nanodisk arrays show a localized plasmon resonance (LSPR), which is a non-propagating mode and appears as a peak in their transmission spectrum.

As an initial step for device performance comparison, we used bulk optical material properties of adhesion layers taken from Ref. 36 for Cr, Ti, and Ta and data taken from Ref. 35 for MgO. The transmission spectra obtained from such simulations are provided in Fig. 5 for all the designed nanostructures. Values of the linewidth increase and resonance magnitude reduction are also calculated from these plots as the percentage difference compared to the case of no adhesion layer (Fig. S1 in the supplementary material). For such calculations, we defined the linewidth as FWHM (full width at half maximum) for the nanohole array and bowtie antenna array. For the nanodisk array, the linewidth is defined as FWHD (full width at half depth) and for the dimer nanohole array as the difference between the resonance wavelength and the wavelength of the nearest adjacent local maximum for the dimer nanohole array. Also, resonance magnitude is defined as the absolute value of the difference between the transmission peak (or dip) and its nearest adjacent local minimum (or maximum).

The results in Figs. 5 and S1 show that magnitude of resonance can decrease by up to %84 and the resonance can broaden up to 2 \times due to Cr adhesion layer losses. However, for the MgO adhesion layer, the reduction in resonance magnitude is less than %3.6 for all the nanostructures, and the linewidth decreases by up to %7, meaning that the resonance becomes even sharper. Furthermore, it can be seen

that for almost all the nanostructures, Ta causes less resonance damping compared to Ti and Cr. The reason is that Ta has a smaller extinction coefficient around the design wavelength. It is important to note that the nanostructure geometry also plays a role in how much the adhesion layer can affect the plasmonic resonance. For example, for the dimer nanohole array, resonance broadening is very small for all adhesion layers, and the reduction in resonance magnitude is the smallest, compared to the other three nanostructures. This is because plasmonic hotspots for the dimer nanohole array have less overlap with the adhesion layer. On the other hand, one can see that the resonance damping is the largest for the nanodisk array, which can be because its gold layer is thinner. These results show that MgO potentially has a much smaller effect on the resonance of plasmonic nanostructures, which makes it a good alternative. However, these results are based on bulk material properties, and experimental estimates should be made by using thin film material data for the adhesion layers.

To provide an experimental estimate for the optical response of the designed nanostructures and compare the effect of the MgO adhesion layer with typical metallic and dielectric adhesion layers, a second set of simulations are performed, which accounts for the small thickness of adhesion layers. For Ta and MgO thin films, we used the ellipsometry measurement results obtained earlier, which are for the same thickness as in the simulations (5 nm). Thin-film material properties of Ti, Cr, and ITO are taken from Refs. 28, 33, and 39, where the optical properties are reported for their thin films. For Cr, the material data are for a thickness of 5 nm, and for Ti and ITO, they are for 32 nm and 17 nm, respectively. Here, we assume that these thin film material properties in Refs. 33 and 39 can be a good estimate for the optical properties of Ti and ITO of 5 nm thickness. It should be noted that, however, the refractive index and extinction coefficient of thin films can be highly changing with their thickness. Furthermore, the deposition method can affect thin film material properties. This is shown in Tables SI, SII, and SIII in the [supplementary material](#) for Cr, Ti, and ITO thin films as an example.

For simulations with adhesion layers considering their thin film material data, the results are provided in Fig. 6. The resonance magnitude reduction and linewidth increase are calculated from these results and plotted in Fig. S2 of the [supplementary material](#). Here, we include the ITO adhesion layer as well since it is also a transparent material, making it an adhesion layer with high optical performance. It can be seen that the previously increasing trend of resonance damping, going from MgO to Ta, Ti, and Cr, is now changed, which is the result of the difference in the thickness and deposition method of the measured thin films. Ta shows the highest plasmonic damping, with up to %84 reduction in resonance magnitude and linewidth broadening of more than two times. MgO, however, still shows up very promising performance in all the cases, causing no resonance broadening (up to %−2) and up to %4 resonance magnitude reduction. Furthermore, one can observe that MgO is as good as ITO in terms of its optical performance, making it a good alternative. Again, the significance of resonance damping in the presence of the adhesion layer depends on the nanostructure geometry and its field distribution at the resonance. For example, resonance broadening is the highest in the case of nanodisk arrays (more than twice) and the plasmonic resonance of the dimer nanohole array is affected the least in the presence of adhesion layer (up to %4 broadening and up to %6 resonance magnitude reduction).

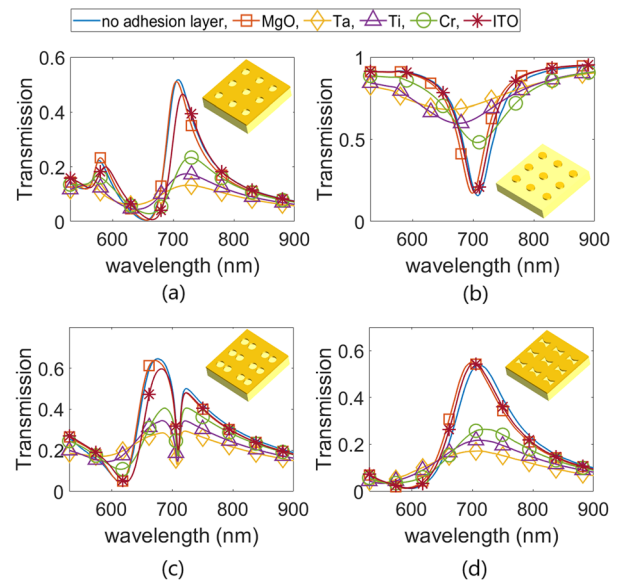


FIG. 6. Transmission spectra without and with different adhesion layers of 5 nm thickness, considering thin film material properties of adhesion materials for (a) nanohole array, (b) nanodisk array, (c) dimer nanohole array, and (d) bowtie slot antenna array.

In summary, MgO is suggested as a lossless alternative adhesion layer for plasmonic nanostructures, to avoid resonance broadening and magnitude reduction caused by common metallic adhesion layers. MgO adhesion tests are performed, demonstrating its strong adhesion. The effect of the MgO adhesion layer on the plasmonic resonance of different nanostructures is compared with Cr, Ti, Ta, and ITO adhesion layers, through FEM simulations. For MgO and Ta specifically, ellipsometry measurements are performed to obtain their thin-film optical properties, which are used in the simulations. The results show that MgO is a promising adhesion layer since it has a negligible effect on the plasmonic resonance of the nanostructures (no resonance broadening and up to %4 resonance magnitude reduction). On the other hand, Ta, Cr, Ti, and ITO broaden the resonance and reduce its magnitude. Although the effect of the adhesion layer is clear, the magnitude of its impact is dependent on the amount of overlap between plasmonic hotspots and the adhesion layer.

See the [supplementary material](#) for additional information on the results in Figs. 5 and 6 and the effect of the thickness and deposition method on optical properties of thin film adhesion layers.

The authors acknowledge support from the Defense Threat Reduction Agency (DTRA) under Grant No. HDTRA1-16-1-0025.

DATA AVAILABILITY

The data that support the findings of this study are available from the corresponding author upon reasonable request.

REFERENCES

1. T. W. Ebbesen, H. J. Lezec, H. F. Ghaemi, T. Thio, and P. A. Wolff, “Extraordinary optical transmission through sub-wavelength hole arrays,” *Nature* **391**, 667 (1998).

- ²C. Escobedo, "On-chip nanohole array based sensing: A review," *Lab Chip* **13**, 2445–2463 (2013).
- ³A. A. Yanik, A. E. Cetin, M. Huang, A. Artar, S. H. Mousavi, A. Khanikaev, J. H. Connor, G. Shvets, and H. Altug, "Seeing protein monolayers with naked eye through plasmonic fano resonances," *Proc. Natl. Acad. Sci. U. S. A.* **108**, 11784–11789 (2011).
- ⁴A. G. Brolo, "Plasmonics for future biosensors," *Nat. Photonics* **6**, 709 (2012).
- ⁵A. Tittl, H. Giessen, and N. Liu, "Plasmonic gas and chemical sensing," in *Nanomaterials and Nanoarchitectures* (Springer, 2015), pp. 239–272.
- ⁶Q. Jiang, B. Rogez, J.-B. Claude, A. Moreau, J. Lumeau, G. Baffou, and J. Wenger, "Adhesion layer influence on controlling the local temperature in plasmonic gold nanoholes," *Nanoscale* **12**, 2524 (2020).
- ⁷C. Jeppesen, N. A. Mortensen, and A. Kristensen, "The effect of Ti and ITO adhesion layers on gold split-ring resonators," *Appl. Phys. Lett.* **97**, 263103 (2010).
- ⁸S. Ekgasit, C. Thammacharoen, F. Yu, and W. Knoll, "Influence of the metal film thickness on the sensitivity of surface plasmon resonance biosensors," *Appl. Spectrosc.* **59**, 661–667 (2005).
- ⁹M. Najiminaini, F. Vasefi, B. Kaminska, and J. J. J. Carson, "Optical resonance transmission properties of nano-hole arrays in a gold film: Effect of adhesion layer," *Opt. Express* **19**, 26186–26197 (2011).
- ¹⁰M. A. Otte, M.-C. Estévez, L. G. Carrascosa, A. B. González-Guerrero, L. M. Lechuga, and B. Sepúlveda, "Improved biosensing capability with novel suspended nanodisks," *J. Phys. Chem. C* **115**, 5344–5351 (2011).
- ¹¹M. Wang, Y. Zhang, X. Zhao, and W. Zhao, "Tunnel junction with perpendicular magnetic anisotropy: Status and challenges," *Micromachines* **6**, 1023–1045 (2015).
- ¹²H. Hughes, K. Bussmann, P. J. McMarr, S. F. Cheng, R. Shull, A. P. Chen, S. Schafer, T. Mewes, A. Ong, E. Chen *et al.*, "Radiation studies of spin-transfer torque materials and devices," *IEEE Trans. Nucl. Sci.* **59**, 3027–3033 (2012).
- ¹³W. M. Abbott, C. P. Murray, C. Zhong, C. Smith, C. McGuinness, E. Rezvani, C. Downing, D. Daly, A. K. Petford-Long, F. Bello *et al.*, "Less is more: Improved thermal stability and plasmonic response in Au films via the use of subnanometer Ti adhesion layers," *ACS Appl. Mater. Interfaces* **11**, 7607–7614 (2019).
- ¹⁴X. Jiao, J. Goeckerit, S. Blair, and M. Oldham, "Localization of near-field resonances in bowtie antennae: Influence of adhesion layers," *Plasmonics* **4**, 37–50 (2009).
- ¹⁵H. Aouani, J. Wenger, D. Gérard, H. Rigneault, E. Devaux, T. W. Ebbesen, F. Mahdavi, T. Xu, and S. Blair, "Crucial role of the adhesion layer on the plasmonic fluorescence enhancement," *ACS Nano* **3**, 2043–2048 (2009).
- ¹⁶N. Djaker, R. Hostein, E. Devaux, T. W. Ebbesen, H. Rigneault, and J. Wenger, "Surface enhanced Raman scattering on a single nanometric aperture," *J. Phys. Chem. C* **114**, 16250–16256 (2010).
- ¹⁷T. G. Habteyes, S. Dhuey, E. Wood, D. Gargas, S. Cabrini, P. J. Schuck, A. P. Alivisatos, and S. R. Leone, "Metallic adhesion layer induced plasmon damping and molecular linker as a nondamping alternative," *ACS Nano* **6**, 5702–5709 (2012).
- ¹⁸M. L. de la Chapelle, H. Shen, N. Guillot, B. Frémaux, B. Guelorget, and T. Toury, "New gold nanoparticles adhesion process opening the way of improved and highly sensitive plasmonics technologies," *Plasmonics* **8**, 411–415 (2013).
- ¹⁹T. Siegfried, Y. Ekinici, O. Martin, and H. Sigg, "Engineering metal adhesion layers that do not deteriorate plasmon resonances," *ACS Nano* **7**, 2751–2757 (2013).
- ²⁰P. Sadri-Moshkenani, M. W. Khan, M. M. Bayer, M. S. Islam, E. Montoya, I. Krivorotov, M. Nilsson, N. Bagherzadeh, and O. Boyraz, "Effect of tantalum and MgO adhesion layers on plasmonic nanostructures," *Proc. SPIE* **11089**, 1108916 (2019).
- ²¹A. G. Brolo, R. Gordon, B. Leathem, and K. L. Kavanagh, "Surface plasmon sensor based on the enhanced light transmission through arrays of nanoholes in gold films," *Langmuir* **20**, 4813–4815 (2004).
- ²²P. Sadri-Moshkenani, M. W. Khan, M. S. Islam, I. Krivorotov, M. Nilsson, N. Bagherzadeh, and O. Boyraz, "Array of symmetric nanohole dimers for STT-RAM ultrathin layer sensing," in *Conference on Lasers and Electro-Optics (CLEO)* (2019).
- ²³H. Guo, T. P. Meyrath, T. Zentgraf, N. Liu, L. Fu, H. Schweizer, and H. Giessen, "Optical resonances of bowtie slot antennas and their geometry and material dependence," *Opt. Express* **16**, 7756–7766 (2008).
- ²⁴I. Zoric, M. Zach, B. Kasemo, and C. Langhammer, "Gold, platinum, and aluminum nanodisk plasmons: Material independence, subradiance, and damping mechanisms," *ACS Nano* **5**, 2535–2546 (2011).
- ²⁵I. Zgura, S. Frunza, M. Enculescu, C. Florica, and F. Cotorobai, "Deposition of titanium dioxide layers upon polyester textile materials: Checking the adherence by ultra-sonication," *Chem. Vap. Deposition* **6**, 9 (2015).
- ²⁶M. Bazargan, M. M. Byranvand, and A. N. Kharat, "A new counter electrode based on copper sheet for flexible dye sensitized solar cells," *Chalcogenide Lett.* **7**, 515–519 (2010).
- ²⁷S. Tigunta, P. Khlikhum, P. Kidkhunthod, N. Chanlek, L. Supadee *et al.*, "Dissolution behavior of MgO thin film-barrier magnetic tunneling junctions," *J. Mater. Sci.* **30**, 6718–6724 (2019).
- ²⁸V. Lozanova, A. Lalova, L. Soserov, and R. Todorov, "Optical and electrical properties of very thin chromium films for optoelectronic devices," *J. Phys.: Conf. Ser.* **514**(1), 012003 (2014).
- ²⁹R. T. Kivaisi, "Optical properties of selectively absorbing chromium films deposited at oblique angle of incidence," *Sol. Energy Mater.* **5**, 115–127 (1981).
- ³⁰L. Jian-ping, L. Li-mei, G. Gui-qing, W. Yang-wei, and L. Fa-chun, "Structural, optical and electrical properties of chromium thin films prepared by magnetron sputtering," *Acta Photonica Sin.* **41**, 922 (2012).
- ³¹M. Khan and S. Haque, "Optical properties of chromium films deposited at normal and oblique angle of incidence," *Phys. Status Solidi A* **136**, K35–K39 (1993).
- ³²S. Mahmoud, "Structure and optical properties of thin titanium films deposited on different substrates," *J. Mater. Sci.* **22**, 3693–3697 (1987).
- ³³P. B. Johnson and R. W. Christy, "Optical constants of transition metals: Ti, V, Cr, Mn, Fe, Co, Ni, and Pd," *Phys. Rev. B* **9**, 5056 (1974).
- ³⁴H. Kangarlou and M. M. Aghgonbad, "Influence of thickness on optical properties of titanium layers," *Opt. Spectrosc.* **115**, 753–757 (2013).
- ³⁵R. E. Stephens and I. H. Malitson, "Index of refraction of magnesium oxide," *J. Res. Natl. Bur. Stand.* **49**, 249–252 (1952).
- ³⁶M. J. Weber, *Handbook of Optical Materials* (CRC Press, 2018).
- ³⁷I. H. Malitson, "Interspecimen comparison of the refractive index of fused silica," *J. Opt. Soc. Am.* **55**, 1205–1209 (1965).
- ³⁸P. B. Johnson and R. W. Christy, "Optical constants of the noble metals," *Phys. Rev. B* **6**, 4370 (1972).
- ³⁹R. J. Moerland and J. P. Hoogenboom, "Subnanometer-accuracy optical distance ruler based on fluorescence quenching by transparent conductors," *Optica* **3**, 112–117 (2016).